Carderock Division
Naval Surface Warfare Center

Bethesda, MD 20084–5000

Finite Element Shock Analysis of a Cryogenic Refrigerator

by

Erwin A. Schroeder
Geoffrey Green

DTIC
SELECTED
MAY 1 7 1995
G
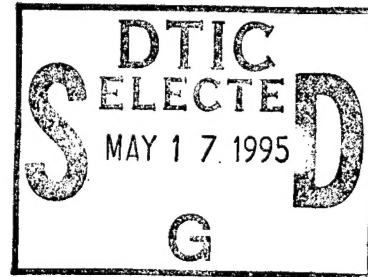
19950516 056

DTIC QUALITY INSPECTED 8

CRDKNSWC/SSD–94–009   Finite Element Element Shock Analysis of a Cryogenic Refrigerator

MAJOR CARDEROCK DIVISION TECHNICAL COMPONENTS

CODE 011 Director of Technology

10 Machinery Systems/Programs and Logistics Directorate

20 Ship Systems and Programs Directorate

50 Hydromechanics Directorate

60 Survivability, Structures and Materials Directorate

70 Signatures Directorate

80 Machinery Research and Development Directorate

90 Machinery In-Service Engineering Directorate

CARDEROCK DIVISION, NSWC, ISSUES THREE TYPES OF REPORTS:

1. **CARDEROCKDIV reports, a formal series,** contain information of permanent technical value. They carry a consecutive numerical identification regardless of their classification or the originating directorate.

2. **Directorate reports, a semiformal series,** contain information of a preliminary, temporary, or proprietary nature or of limited interest or significance. They carry an alphanumerical identification issued by the originating directorate.

3. **Technical memoranda, an informal series,** contain technical documentation of limited use and interest. They are primarily working papers intended for internal use. They carry an identifying number which indicates their type and the numerical code of the originating directorate. Any distribution outside CARDEROCKDIV must be approved by the head of the originating directorate on a case-by-case basis.

REPORT DOCUMENTATION PAGE

1a. REPORT SECURITY CLASSIFICATION	1b. RESTRICTIVE MARKINGS
UNCLASSIFIED	

2a. SECURITY CLASSIFICATION AUTHORITY	3. DISTRIBUTION/AVAILABILITY OF REPORT
	Approved for public release; distribution is unlimited.
2b. DECLASSIFICATION/DOWNGRADING SCHEDULE	

4. PERFORMING ORGANIZATION REPORT NUMBER(S)	5. MONITORING ORGANIZATION REPORT NUMBER(S)
CRDKNSWC/SSD−94−009	

6a. NAME OF PERFORMING ORGANIZATION	6b. OFFICE SYMBOL	7a. NAME OF MONITORING ORGANIZATION
Carderock Division Naval Surface Warfare Center	Code 2042	Carderock Division Naval Surface Warfare Center (Code 812)

6c. ADDRESS (City, State, and ZIP Code)	7b. ADDRESS (CITY, STATE, AND ZIP CODE)
Bethesda, MD 20084-5000	3A Leggett Circle Annapolis, MD 21402−5067

8a. NAME OF FUNDING/SPONSORING ORGANIZATION	8b. OFFICE SYMBOL	9. PROCUREMENT INSTRUMENT IDENTIFICATION NUMBER
Program Executive Office Mine Warfare	PMO 407−7	

8c. ADDRESS (City, State, and ZIP Code)	10. SOURCE OF FUNDING NUMBERS			
	PROGRAM ELEMENT NO.	PROJECT NO.	TASK NO.	WORK UNIT ACCESSION NO.
2531 Jefferson Davis Hwy Arlington, VA 22242−5167	63555N	S2142MW	S2141−904	12712300

11. TITLE (Include Security Classification)

Finite Element Element Shock Analysis of a Cryogenic Refrigerator

12. PERSONAL AUTHOR(S)

Erwin A. Schroeder, Geoffrey Green

13a. TYPE OF REPORT	13b. TIME COVERED		14. DATE OF REPORT (Year, Month, Day)	15. PAGE COUNT
Interim	FROM 1/93	TO 8/93	December 1994	24

16. SUPPLEMENTARY NOTATION

17. COSATI CODES			18. SUBJECT TERMS (Continue on reverse if necessary and identify by block number)
FIELD	GROUP	SUB−GROUP	Cryogenic Rrefrigeration Superconducting Systems Shock Aanalysis Finite Element

19. ABSTRACT (Continue on reverse if necessary and identify by block number)

Two-stage Gifford-McMahon refrigerators are candidates for use in cooling superconducting magnets for naval applications in mine countermeasures and electric-drive propulsion for ships. For these applications, the refrigerators can be expected to undergo shock and vibration due to the motion of the platform on which they are mounted and to explosions of nearby mines. If the refrigerator is to continue operating effectively, the cylinder walls must not be permanently deformed when subjected to shock loads, and therefore stresses in the walls must not approach the elastic limit of the wall material. The stress in the cylinder walls due to specified shocks was determined by an axisymmetric finite element shock analyses of the two-stage cylinder and displacer assembly. For this analysis, it was assumed that the displacers were at the bottom of their stroke and each was resting on the bottom of its cylinder. Constant horizontal and vertical accelerations of 100 g and a time-dependent acceleration with maximum amplitude of 103 g were applied to the model. The analysis for the vertical shock loading produced a maximum stress of 36.7 MPa, 5 percent of yield for the 304-type stainless steel used for the cylinder walls.   (continued on reverse)

20. DISTRIBUTION/AVAILABILITY OF ABSTRACT	21. ABSTRACT SECURITY CLASSIFICATION
[X] UNCLASSIFIED/UNLIMITED ☐ SAME AS RPT. ☐ DTIC USERS	UNCLASSIFIED

22a. NAME OF RESPONSIBLE INDIVIDUAL	22b. TEL. (include Area Code)	22c. OFFICE SYMBOL
Erwin A. Schroeder	(301) 227−1660	Code 2042

DD FORM 1473

Block 19. (continued)

The horizontal shock loading produced a maximum stress of 144 MPa, 19 percent of yield for the stainless steel.
The time-dependent analysis produced a maximum stress of 18.4 MPa, 2 percent of yield for the stainless steel.
These stress values are consistent with the expectation that a constant acceleration will produce larger stresses
than a time-varying acceleration of equal maximum amplitude that does not excite a resonance of the structure.
Given the anticipated values of horizontal and vertical shock to be applied during testing, it is expected that the
refrigerator will not experience damaging strain.

Accesion For	
NTIS CRA&I	X
DTIC TAB	☐
Unannounced	☐
Justification	
By	
Distribution /	
Availability Codes	
Dist	Avail and / or Special
A-1	

CONTENTS

FIGURES

TABLES

ABSTRACT

Two-stage Gifford-McMahon refrigerators are candidates for use in cooling superconducting magnets for naval applications in mine countermeasures and electric-drive propulsion for ships. For these applications, the refrigerators can be expected to undergo shock and vibration due to the motion of the platform on which they are mounted and to explosions of nearby mines. If the refrigerator is to continue operating effectively, the cylinder walls must not be permanently deformed when subjected to shock loads, and therefore stresses in the walls must not approach the elastic limit of the wall material. The stress in the cylinder walls due to specified shocks was determined by an axisymmetric finite element shock analyses of the two-stage cylinder and displacer assembly. For this analysis, it was assumed that the displacers were at the bottom of their stroke and each was resting on the bottom of its cylinder. Constant horizontal and vertical accelerations of 100g and a time-dependent acceleration with maximum amplitude of 103g were applied to the model. The analysis for the vertical shock loading produced a maximum stress of 36.7 MPa, 5 percent of yield for the 304-type stainless steel used for the cylinder walls. The horizontal shock loading produced a maximum stress of 144 MPa, 19 percent of yield for the stainless steel. The time-dependent analysis produced a maximum stress of 18.4 MPa, 2 percent of yield for the stainless steel. These stress values are consistent with the expectation that a constant acceleration will produce larger stresses than a time-varying acceleration of equal maximum amplitude that does not excite a resonance of the structure. Given the anticipated values of horizontal and vertical shock to be applied during testing, it is expected that the refrigerator will not experience damaging strain.

INTRODUCTION

The U.S. Navy is investigating applications of superconducting magnet technology for use in mine countermeasures and electric drive propulsion for ships. Two-stage Gifford-McMahon refrigerators are likely candidates for
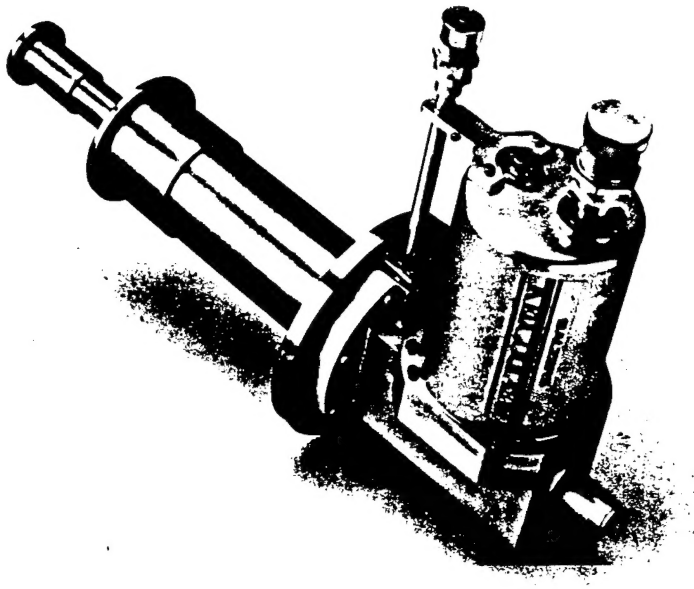
1

Figure 1. Balzers Model UCH-130 Gifford-McMahon refrigerator

cooling the magnets in these applications.[1,2] * Figure 1. shows a photograph of a Balzers Model UCH-130 Gifford-McMahon refrigerator of the type analyzed here. For each stage in this Gifford-McMahon design, the regenerative heat exchanger, subsequently referred to as a regenerator, is located inside the displacer resulting in the addition of non-structural mass to the displacer.

For naval applications, these refrigerators can be expected to undergo shock and vibration due to the motion of the platform on which they are mounted. In mine-sweeping applications, nearby mine explosions may produce additional shocks. If the refrigerator is to continue operating effectively after experiencing shock loads, the cylinder walls must not be permanently deformed, and therefore the wall material must not approach its elastic limit when subjected to these loads. The goal of this work is to determine the stress in the cylinder walls due to expected shocks by making shock analyses of the cylinders of the two-stage cylinder and displacer assembly. The cylinders and displacers were modeled with finite elements and constant 100 g horizontal and vertical accelerations and a time-dependent acceleration having a 103 g maximum amplitude were applied to the model. The resulting displacements and stresses were plotted, and the maximum values of each were extracted.

This report documents the modeling assumptions, details, and results produced by the analyses. Appendix A contains diagrams of the refrigerator components represented by the finite element model and Appendix B contains representative displacement and stress plots.

* The references are listed on page 23.

2

MODELING ASSUMPTIONS

A two-stage Gifford-McMahon refrigerator mounted in a vacuum vessel was analyzed using the finite element method to determine its mechanical response to shock loading. Since determining the effect of shock on the vacuum vessel is outside the scope of this work, the prescribed shock acceleration was assumed to be that transferred to the refrigerator by the vessel and was applied at the top of the first stage where the refrigerator is attached to the vessel. To obtain the effect of a constant acceleration produced by a force applied at the top of the first stage, the motion of the top of the first stage was constrained and a gravitational acceleration in the direction opposite to the shock acceleration was applied to the structure. Figure 3. in Appendix A shows the location at which the acceleration loading was applied. Displacements and stresses produced by vertical accelerations parallel to the geometric axis of the cylinders and horizontal accelerations perpendicular to the axis were determined using finite element analyses. The vertical and horizontal accelerations were applied in separate computer runs. Since the assembly of the first- and second-stage cylinders and displacers of the refrigerator is rotationally symmetric with respect to the central axis, the assembly was modeled using axisymmetric finite elements. A three-dimensional axisymmetric structure is generated by rotating a two-dimensional region around an axis of symmetry and an axisymmetric analysis models the structure by subdividing this two-dimensional region. Since the subdivided region was two-dimensional, the analysis used fewer elements and was less costly to run than one using a full three-dimensional model. For this analysis, the two-dimensional region was subdivided into triangles and quadrilaterals. In an axisymmetric analysis, nonaxisymmetric loads can be applied to an axisymmetric structure by expressing them as Fourier expansions in the azimuthal angle. However, if a nonaxisymmetric loading produces nonlinear effects, it may introduce non-physical effects. For example with horizontal accelerations, the effect of the interface between the cylinder and displacer is nonlinear, since where the surface is in compression, there are action and reaction forces between the cylinder and displacer, but where the surface is in tension there are no forces between them. In an axisymmetric analysis the interface is either connected or disconnected at all azimuthal angles. It was assumed that these effects did not significantly influence the results.

The cold head at the lower end of the first-stage cylinder fits into the first-stage cylinder wall. The cold head is joined to the cylinder wall by a weld that was estimated to connect the lower one-fourth of the surface between the two pieces. See Appendix A for a sketch of the weld detail. For horizontal accelerations it was assumed that the cold head fits snugly in the cylinder and the relative normal motion of the surfaces was constrained where they were in contact but not welded. For the region where the surfaces were in compression this was a physically realistic constraint, but for the region where these surfaces tended to separate, it was not. The finite element analysis showed that for vertical acceleration, these surfaces tended to separate around the cylinder, so no constraint on relative normal motion was applied for this case.

3

A motor drives the displacers through a scotch-yoke mechanism. To avoid modeling the driving mechanism, the analysis was limited to the situation in which, at the time of the shock, the displacers were at the lowest point in the cycle so that each was resting on the bottom of its cylinder. For vertical acceleration, maximum load on the cylinders and thus maximum stress occurs when the displacers are resting on the bottom of the cylinders. For horizontal acceleration, the moment of inertia about the attachment of the refrigerator to the vacuum vessel is largest when the displacers are at the bottom of the cylinders and also produces maximum stress in the cylinders. It was also assumed that there was sufficient slack in the connection joining the two displacers that they could be assumed to have been not connected.

The displacer of each stage in this design of the Gifford-McMahon refrigerator contains a regenerator, a cavity filled with heat-absorbing material that contributes to the mass of the displacer, but does not contribute to its strength. Structural mass contributes significantly to the stiffness of the object and is represented by finite elements; when this material is assigned a mass density, the finite element program automatically computes its contribution to the mass matrix. Non-structural mass makes at most an insignificant contribution to the structural stiffness and therefore is not modeled with finite elements. Non-structural mass is combined with the structural mass of adjacent elements and in this analysis was included by an appropriate increase in the density assigned to the material of these elements. The structural part of each displacer was modeled with finite elements leaving a cavity for the regenerator. The mass of the regenerator material was determined and a layer of finite elements on the surface of the cavity was assigned a density that accounted for the layer's mass and the non-structural mass of the heat-absorbing material. For horizontal acceleration, the non-structural mass was assigned to the layer of elements on the side of the cavity to represent horizontal inertia and for vertical accelerations, the non-structural mass was assigned to the layer of elements on the bottom of the cavity to represent vertical inertia.

Normal motion on the surfaces between the displacers and cylinders was constrained and tangential motion between these surfaces was not constrained. With axisymmetric modeling, this assumption implied that for horizontal loading the displacer pushed on the cylinder wall if its relative motion was toward it, but it also implied that the displacer pulled on the wall if its relative motion tended to be away from the wall. The first implication was physically realistic; the second was not. For vertical loading these constraints caused no problem.

The material property data were obtained for the three structural materials represented in the analysis; copper and type 304 stainless steel which form the cylinders, and a cotton-phenolic composite which forms the displacers. Where temperature dependent data were available, data for the 4K operating temperature of the refrigerator were chosen. Table 1. gives material property values for three temperatures and for the values used in the finite element

Table 1. Material Property Values

Stainless Steel 304					
	Used	19K	30K	300K	Reference
Youngs Modulus – GPa	199.	199.	200.	192.	Figure B.4.i[3]
Shear Modulus – GPa	76.5	76.5	78.9	73.6	Figure B.2.l[3]
Density – Kg/M^3	7851.				
Copper					
	Used	4K	30K	300K	Reference
Youngs Modulus – GPa	139.	139.	139.	128.	Table 1.2[3]
Shear Modulus – GPa	51.7	51.7	51.7	47.6	Table 1.3[3]
Density – Kg/M^3	8960.·				
Cotton-Phenolic Composite				Reference	
Youngs Modulus – GPa	6.27			NEMA Grade: LE	
Shear Modulus – GPa	2.14			General Electric Grade: 1841	
Density – Kg/M^3	1335.			Mil Spec 15035FBE	

analyses. Because densities for stainless steel and copper were used to determine the mass of the finite elements, and the dimensions of the structure are the dimensions at room temperature, the densities at room temperature gave correct mass values. The elasticity data for stainless steel and copper were taken from the *Cryogenic Materials Data Handbook*.[3] The value of Young's modulus, E was obtained from the "Annealed" curve in fig B.4.i. The equation $G = E/2(1 + v)$, with $v = 0.3$ determined the shear modulus, G. The data for the composite was taken from General Electric data sheets for cotton-phenolic composite designated NEMA Grade: LE, General Electric Grade: 1841, MilSpec 15035FBE. From Young's modulus, the preceding equation determined G also for the composite. In some cases for the three materials values and significant figures were estimated from plots.

FINITE ELEMENT MODEL

An axisymmetric structure is a structure that is rotationally symmetric about an axis and whose shape can be generated by rotating a two-dimensional plane area around the axis. A finite element model for an axisymmetric structure can be made by dividing the generating plane area into finite subregions or elements. The boundaries of the finite elements consist of lines or curves through points, called nodes, in the plane area. Thus the nodes represent grid circles generated by the points as they are rotated about the axis of symmetry, and the elements represent solid rings generated by the rotated areas. The finite elements used to model the refrigerator are the NASTRAN axisymmetric

triangle TRIAAX with three nodes, and the axisymmetric trapezoid TRAPAX with four corner nodes.[4] These elements approximate the continuous displacement field inside the element by linear functions that interpolate between displacements at the nodes. Both axisymmetric and non-axisymmetric loads can be applied to these elements to produce axisymmetric and non-axisymmetric displacements and stresses. Non-axisymmetric loads and displacements are expanded in harmonic series and the coefficients in the series become the finite element unknowns. The vertical acceleration was applied as an axisymmetric load and the horizontal acceleration load was applied as a non-axisymmetric one-term cosine series. For axisymmetric loading or at most a horizontal acceleration, the displacements are of the form:

$$
\begin{array}{lll}
\text{radial} & \Delta r_0 & + & \Delta r_1 \cos\phi \\
\text{azimuthal} & & & \Delta a_1 \sin\phi \\
\text{axial} & \Delta z_0 & + & \Delta z_1 \cos\phi
\end{array}
$$

For axisymmetric loading, the terms involving ϕ do not appear.

Since the cylinder walls are thin compared to their length, a large number of elements was needed for the model. To represent bending adequately, four elements through the thickness of the cylinder walls were used. To obtain a well-conditioned system of equations, the ratio of the longest to shortest side should be less that 1.5. These two requirements determined the number of elements in the cylinder walls. Constraints linking grid points on the cylinder walls with corresponding points on the displacers also determined the number of elements in the displacers.

A refined mesh accommodated the larger stresses expected in the region of the weld that joins the two stages. A mesh generation program written for this model produced the major part of the finite element grid. The refined mesh in the region of the weld and the elements representing the curved surface at the top of the second stage was added by hand. The complete model contained 23350 elements connecting 25011 grid points. The figures in Appendix B show the finite element grid used.

FINITE ELEMENT ANALYSIS

This section provides a brief outline of the finite element method as it applies to this problem. The description follows the NASTRAN Theoretical Manual, Section 5.ll[4] which can be consulted for the details of the method. The finite element analysis approximates the continuous displacement field in a deformed structure by a set of displacement values at a finite number of locations or nodes in the structure. It determines the set of these displacements that produces the minimum potential energy of the system consisting of the deformed structure and the forces producing the deformation. The displacement values at the nodes of the finite element model are the components of a displacement vector $\{u\}$. The approximation produces a system of linear equations which is solved for the displacements at the nodes.

The energy associated with a displaced structure is the sum of the strain energy U of the elastic deformation and the displacement energy W of the loads.

$$U + W = \frac{1}{2} \int_S \sigma \epsilon \, dV + \int_S F_{\lambda} \cdot u \, dV$$

where in the volume S occupied by the structure

σ is the stress field,

ϵ is the strain field,

u   is the displacement field, and

F_{λ} is the external force field.

The preceding equation must be expressed as the finite element matrix equation $[K]\{u\} = -\{F_{\lambda}\}$, a system of linear equations where $[K]$ is a matrix that represents the stiffness of the structure, $\{F_{\lambda}\}$ is the vector of acceleration forces, and $\{u\}$ is the vector of the unknown nodal displacements. The analysis was made using the NASTRAN finite element program.

The system of linear equations that determines the displacements at the nodes of the finite element model is the sum of systems of equations for the individual elements. The following description of the analysis is given for one triangular element with its three nodes designated a, b, and c. The derivation for the trapezoidal element is similar, with four nodes in place of the three. In the analysis of axisymmetric structures with nonsymmetric loads, the displacements and loads are represented as Fourier expansions in series of sine and cosine terms of the azimuthal angle ϕ. The degrees of freedom are harmonic coefficients of the displacement components. The special case of acceleration loading needs only the zeroth and first terms. With a vertical axis of symmetry the zeroth harmonic displacements for vertical acceleration are:

$$
\begin{aligned}
u &= u_0(r, z) \quad \text{radial} \\
v &= 0 \quad\quad\quad \text{azimuthal} \\
w &= w_0(r, z) \quad \text{axial}
\end{aligned}
$$

and the first harmonic displacements for horizontal acceleration are:

7

$$u = u_1(r, z) \cos \phi \quad \text{radial}$$
$$v = v_1(r, z) \sin \phi \quad \text{azimuthal}$$
$$w = w_1(r, z) \cos \phi \quad \text{axial}$$

The linear functions of the radial and axial coordinates r and z that approximate the displacement field in each element are

$$u = \beta_1 + \beta_2 r + \beta_3 z$$
$$v = \beta_4 + \beta_5 r + \beta_6 z$$
$$w = \beta_7 + \beta_8 r + \beta_9 z$$

For a triangular element, the components of displacement at its three nodes a, b, and c are: u_a, v_a, w_a, u_b, v_b, w_b, u_c, v_c, w_c and these displacements are included among the components of the vector $\{u\}$ and are the components of a vector designated $\{u^e\}$.

The vector of strains for the n = 0, 1 harmonics are:

$$\{\epsilon_n\} = \left\{ \begin{array}{c} \dfrac{\partial u_n}{\partial r} \\[6pt] \dfrac{\partial w_n}{\partial z} \\[6pt] \dfrac{n}{r} v_n + \dfrac{u_n}{r} \\[6pt] \dfrac{\partial u_n}{\partial r} \\[6pt] -\dfrac{n}{r} u_n + \dfrac{\partial v_n}{\partial r} - \dfrac{v_n}{r} \\[6pt] \dfrac{\partial v_n}{\partial z} - \dfrac{n}{r} w_n \end{array} \right\} \approx [H^n_{\epsilon\beta}(r, z)]\{\beta\}$$

The matrix $[H^n_{\epsilon\beta}(r, z)]$ is obtained using the linear approximation of the displacement field and is a function of the position coordinates r and z and the harmonic parameter n. $\{\beta\}$ is a vector with components $\beta_1, \ldots, \beta_9$. Now the vector $\{\beta\}$ must be expressed in terms of the displacement vector $\{u\}$.

Since the individual harmonics are independent, each can be analyzed independently. Subsequently, the subscript n designating the displacement harmonic is suppressed in favor of a subscript i designating the displacement at the ith node of an element. The linear approximation applied to the three nodal points (r_i, z_i) for i = a, b, c of the triangular finite element produces the transformation:

8

$$\begin{Bmatrix} u_i \\ v_i \\ w_i \end{Bmatrix} = \begin{Bmatrix} \beta_1 + \beta_2 r_i + \beta_3 z_i \\ \beta_4 + \beta_5 r_i + \beta_6 z_i \\ \beta_7 + \beta_8 r_i + \beta_9 z_i \end{Bmatrix}$$

Using these transformations, the vector $\{\beta\}$ and the vector $\{u^e\}$ with components $u_a, v_a, w_a, \ldots, w_c$ we define the inverse of the matrix $[H_{\beta u}]$, determined only by the coordinate locations of the element nodes, by:

$$\{u^e\} = [H_{\beta u}^{-1}]\{\beta\} \qquad \text{so that} \qquad \{\beta\} = [H_{\beta u}]\{u^e\}$$

The strain field is now approximated in terms of the vector of displacements by:

$$\{\epsilon_n\} = [H_{e\beta}^n(r, z)][H_{\beta u}]\{u^e\}$$

and the stress vector is given by:

$$\{\sigma\} = [E]\{\epsilon\}$$

where the matrix $[E]$ depends only on Young's modulus and the Poisson's ratio. Now in each element, the stress field is approximated by:

$$\{\sigma^e\} = [E][H_{e\beta}^n(r, z)][H_{\beta u}]\{u^e\}$$

where $\{\sigma^e\}$ is the restriction of the stress vector to the elements nodal points.

Since the components of the vector $\{u^e\}$ are are included among the components of $\{u\}$, the transformation matrix $[H_{\beta u}]$ can be extended to a transformation of $\{u\}$ and the expressions for $\{\epsilon^e\}$ and $\{\sigma^e\}$ can be extended to $\{\epsilon\}$ and $\{\sigma\}$. In terms of nodal displacements, the strain energy of the displaced structure is approximated by:

$$U = \frac{1}{2} \sum_{\text{elements}} \{u\}^T \int [H_{\beta u}]^T [H_{e\beta}^n(r, z)]^T [E][H_{e\beta}^n(r, z)][H_{\beta u}]dV \{u\}$$

$$= \frac{1}{2} \{u\}^T [K]\{u\}$$

The stiffness matrix $[K]$ and the displacement vector $\{u\}$ form the first term of the finite element matrix equation. The force vector remains to be obtained.

The mass of an element having area A, radial distance to its centroid r_o, and density ϱ is $M = 2\pi\varrho r_o A$. Each node of a triangular element is assigned one-third of the element's mass and each node is assigned the sum of the masses for all elements attached to the node. If the mass assigned to a node is m_j where the index j ranges over all nodes in the

9

finite element model and if the node is subjected to an acceleration $\mathcal{A}$, the component of force applied to the node is $m_j\mathcal{A}$. The potential energy of acceleration forces on the displaced structure is

$$W = \{F_\mathcal{A}\} \cdot \{u\}$$

Where $\{F_\mathcal{A}\}$ is the vector of acceleration forces on the structural nodes. For equilibrium, the derivatives of the total potential energy with respect to the individual displacements must vanish

$$\frac{\partial}{\partial\{u\}}(U + W) = [K]\{u\} + \{F_\mathcal{A}\} = 0$$

This is the system of linear equations that forms the finite element matrix equation and is solved for the displacements at the nodes of the finite element model. In most cases, this system requires adjustments to reflect boundary conditions, constraints, etc.[4]

ANALYSIS RESULTS

Three types of analyses were made using the finite element model. Those of the first type were analyses of applications of constant 100g accelerations applied separately in the vertical and horizontal directions. Displacements and stresses produced by these loads were plotted. The second type was an analysis of an application of a time-dependent vertical acceleration at the top of the first stage. For the time-dependent acceleration, the maximum stress components were identified and the accelerations at the lower end of the first and second stages were plotted. The third type was a determination of natural vibration frequencies of the refrigerator with the top of the first stage mounted on fixed flange. The refrigerator was oriented with its axis of symmetry vertical and with the first stage at the top (see Figure 3. in Appendix A). The acceleration loads were applied at the top of the first stage where the refrigerator is attached to the vacuum container. The goal of this work was to determine whether stresses in the cylinders of the two stages would remain below the elastic limit, so only stresses in the cylinders were computed and examined.

Constant Acceleration Case

In the NASTRAN model for the constant acceleration case, the acceleration load was applied by constraining the top of the first stage and applying a constant gravitational acceleration of 100g to all elements in the model. Two loading cases of 100g acceleration each were applied to the model. The first load was applied in the vertical direction and the second in the horizontal direction. The resulting displacements and stresses were plotted for each case. Appendix B contains examples of these plots. Table 2. shows the maximum absolute value of the stresses for each loading case and each stress orientation. The stresses observed were less than the yield stress, 785 MPa for cold rolled tempered 304 stainless steel.[5]

Table 2. Maximum Time-Independent Stresses

Vertical Acceleration — 100g	
Radial Stress — MPa	11.4
Axial Stress — MPa	36.7
Circumferential Stress — MPa	16.5
Shear Stress — RZ — MPa	11.1
Horizontal Acceleration — 100g	
Radial Stress — MPa	37.8
Axial Stress — MPa	143.5
Circumferential Stress — MPa	83.1
Shear Stress — RZ — MPa	36.8

Displacements for grid points on the cylinders were plotted and printed. Table 3. gives the maximum displacements for the two loading cases. The maximum radial displacement for the horizontal case occurs at points on the bottom of the second stage lying on the plane defined by the center of the cylinder and the displacement vector; the maximum azimuthal displacement occurs on the cylinder 90 degrees from these points. The values of these maximum horizontal displacements are equal.

Table 3. Maximum Time-Independent Displacements

Vertical Acceleration — 100 g		
Component	Value — mm	Location
Radial	.0001	Bottom of Stage 1
Axial	.0172	Bottom of Stage 2
Horizontal Acceleration — 100g		
Component	Value — mm	Location
Radial	.5715	Bottom of Stage 2
Azimuthal	.5715	Bottom of Stage 2
Axial	.0787	Bottom of Stage 2

Table 4. Natural Frequencies of the Refrigerator

Frequencies (Hz)	Period (sec)
1324	0.00076
2400	0.00042
3108	0.00032

Natural Frequencies of the Refrigerator

An eigenvalue solution of the finite element matrix equation gives the natural frequencies of the modeled structure. Table 4. shows the natural frequencies of the refrigerator model and the corresponding periods of the vibrations.

Time-Dependent Acceleration Case

The time-dependent acceleration data were taken from the curve "Lightweight Test, Top Blow" in Figure 15 in Bradley et al[6]. This curve gives the vertical acceleration at the test machine. The maximum amplitude of this acceleration was 103 g. In the NASTRAN model for this case, the time-dependent acceleration load was applied to the top of the first stage. Since transient analyses produces a large amount of data for each node selected, stresses were selected to be computed only at nodes in regions that showed high stress values in the static case. Table 5. gives the time, location, and value of the maximum stresses at these nodes.

The time-history of the accelerations at the bottom flanges of the two stages were computed. Figure 2. shows the vertical acceleration applied at the flange of the vacuum vessel and the vertical components of the computed acceleration at the two stages. The radial and axial components of the computed accelerations were small compared to the vertical components. The curves in Figure 2. show that the input acceleration changes slowly relative to the period of the lowest natural frequency and therefore the response follows the applied acceleration closely. The frequency content of the applied acceleration does not approach resonance and the maximum response amplitude was smaller than that of the constant acceleration.

CONCLUSIONS

The maximum stress produced by the analysis for vertical steady state shock loading was 36.7 MPa (from Table 2.). This value was 5 percent of yield for tempered stainless steel. The maximum stress produced for horizontal shock loading was 143.5 MPa which is 19 percent of yield. This stress was closer to the yield value, however it is believed that any horizontal shocks experienced by this equipment will be much less than the assumed 100 g. The maximum stress
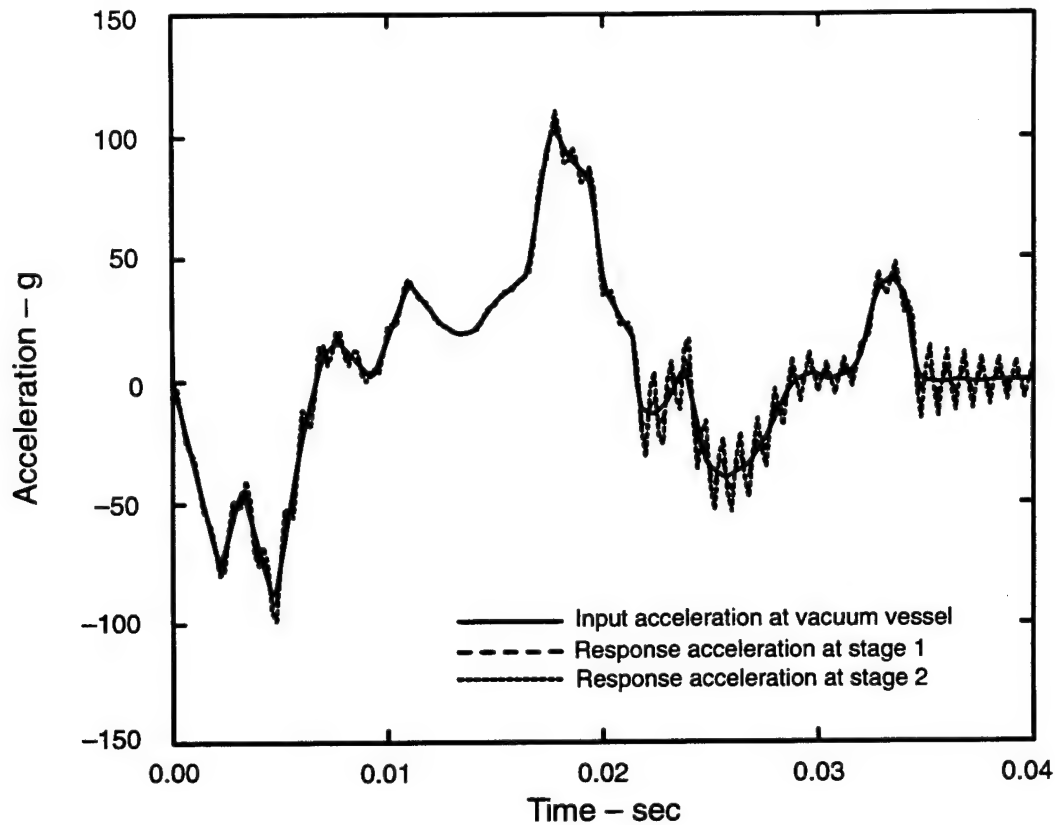
12

Figure 2. Transient analysis – computed accelerations

Table 5. Maximum Time-Dependent Stresses

Stress Component	Time seconds	Max Stress MPa	Location
Radial	0.018	5.16	Stage 1 cylinder wall, near top of weld
Axial	0.018	18.4	Stage 1 cylinder wall, near top of weld
Circumferential	0.018	14.2	On curved radius, near top of Stage 2
Shear	0.018	5.58	On curved radius, near top of Stage 2

found in the time-dependent analysis was 18.4 MPa (from Table 3.) which is 2 percent of yield. Comparison of the natural frequencies in Table 4. with the curves in Figure 2. shows that the time varying acceleration applied to the structure changed slowly compared to the period of its natural frequency. Therefore the time varying acceleration did not excite a resonance in the structure and produced smaller stresses than the constant acceleration of similar maximum amplitude. As a result of these analyses, given the anticipated values of horizontal and vertical shock during testing, it is expected that the refrigerator will not experience damaging strains.

13

APPENDIX A – SKETCHES OF CYLINDERS AND DISPLACERS

Figure 3. is a sketch of the cross section of the first- and second-stage cylinders; it gives the dimensions used in the finite element model. Figure 4. is a sketch of the displacers showing the dimensions used. The detail of the welded joint between the two stages is shown in Figure 5. The depth of the weld is assumed to equal 1.65 mm. The surfaces that are welded are assumed to be in contact in the region that is not welded. Because of expected stress concentrations near the top of the weld, the finite element model was refined in the region of the weld.
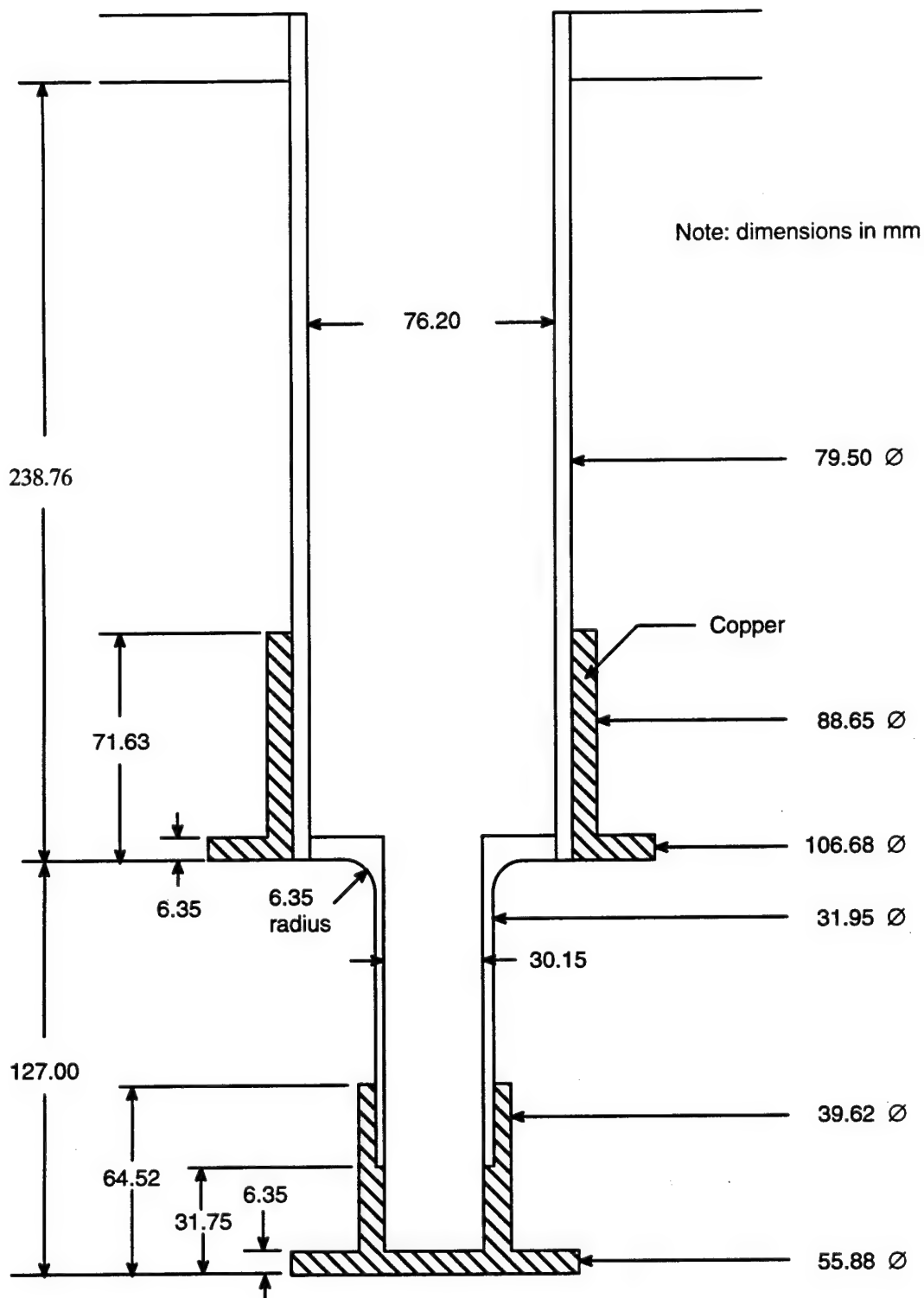
Note: dimensions in mm

76.20

238.76

79.50 Ø

Copper

71.63

88.65 Ø

106.68 Ø

6.35

6.35
radius

31.95 Ø

30.15

127.00

39.62 Ø

64.52

6.35

31.75

55.88 Ø

Figure 3. First and Second Stage Cylinders (approximately to scale)

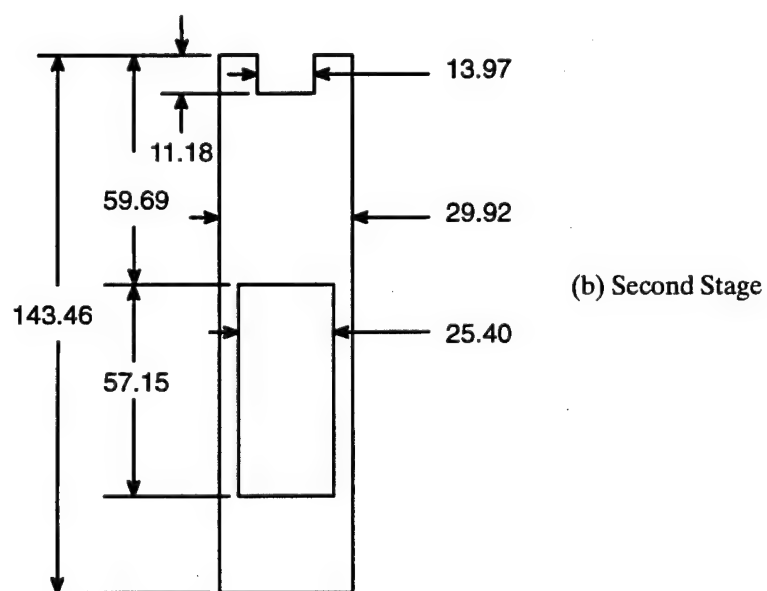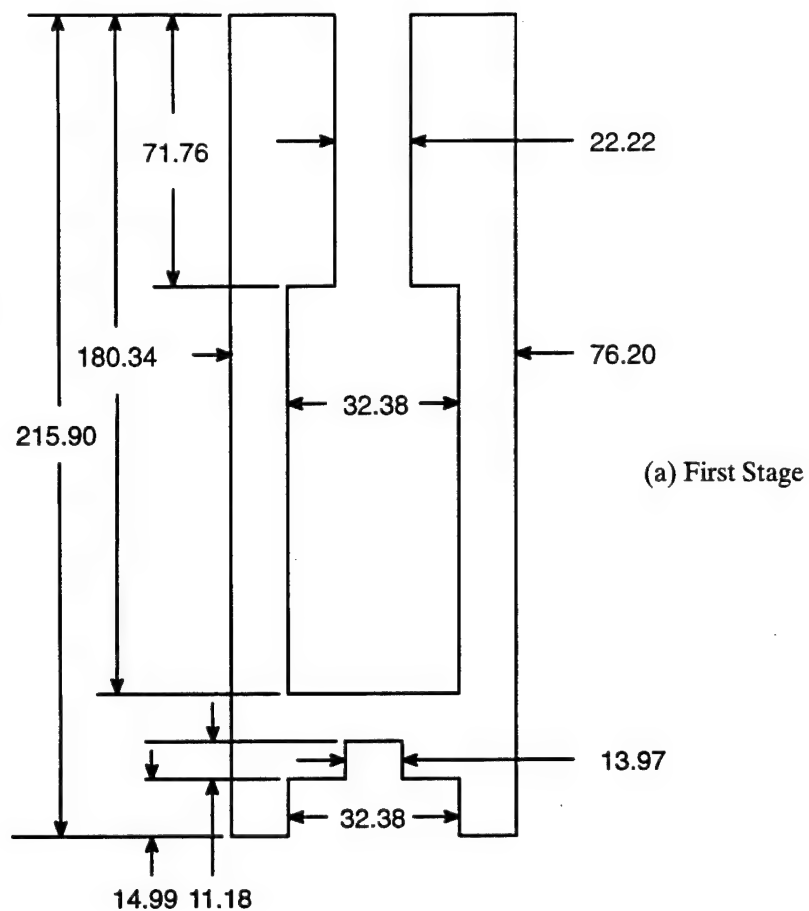Note: dimensions in mm

(a) First Stage

(b) Second Stage

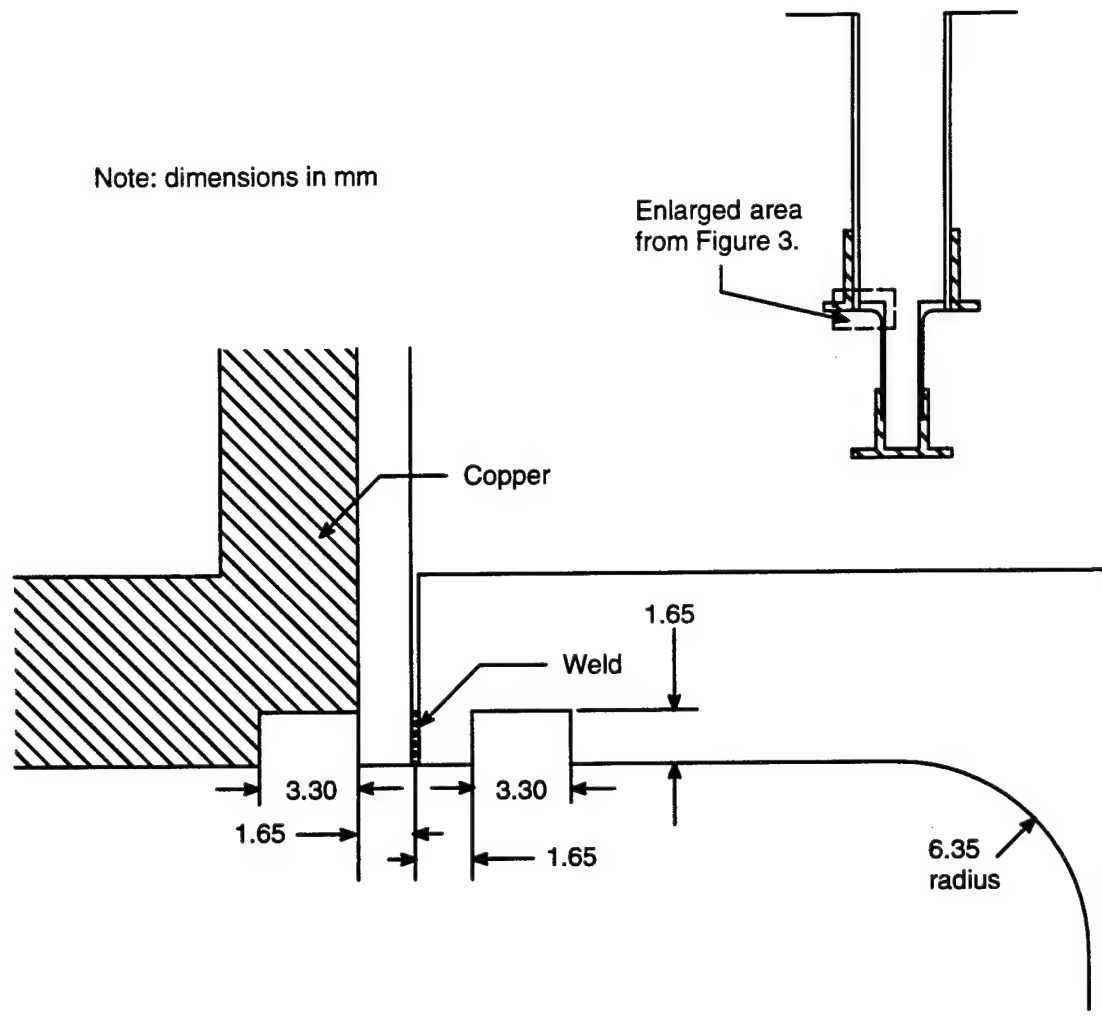Figure 4. First and Second Stage Displacers (approximately to scale)

16

Figure 5. Detail of the Welded Joint

APPENDIX B – PLOTS OF DISPLACEMENTS AND STRESS LEVELS

Plots were made showing the displacements and stresses produced by the finite element analyses. This appendix includes plots of the undeformed and deformed finite element meshes and color stress level plots for the displacement components having the largest stresses for each of the shock loading cases that were run. Figure 6. shows the undeformed finite element model for the cylinders for the two stages and the deformed plots for the horizontal and vertical shock loading. Individual elements are not visible in this figure because of the large number of elements. Since the maximum displacements in the horizontal and vertical cases were of the order of 0.02 mm and 0.57 mm respectively, the plotted displacements are greatly exaggerated to be visible. Figure 7. shows enlargements of the displacement plot for the vertical acceleration for the region in which the two stages are joined, the lower end of stage one and the upper end of stage two. These enlarged plots show the refinement in the finite element grid for the region near the weld. Even though the displacements were very small, it is evident that the largest distortions were in the vicinity of the weld and the connection between the first and second stages.

Color plots showing the stress levels in the cylinder walls were made for all of the stresses shown in Table 2. For each component, one plot shows the stress levels in the complete finite element model. The other plot is an enlargement of the region which connects the two stages. This region contains the welded joint that joins the two stages and the curved section that fairs the lower end of the first stage into the wall of the second stage. These two locations produce some of the higher stress values experienced in the analyses. Figure 8. and Figure 9. are plots of the axial stress, the largest stress components for the horizontal and for vertical shock accelerations. For the horizontal acceleration, Figure 8. shows that the stresses in the vertical direction were largest where the bending moments are largest, at the top of the first- and second-stage cylinders. These axial stresses were due to compression on one side of the cylinder and tension on the other. There were also axial stress concentrations near the top of the weld that joins the first and second stages. Figure 9. shows axial stress levels for the vertical acceleration case. In this axisymmetric case, axial stress was due to stretching or in some locations compression which was uniform around the cylinder. The largest stress concentrations were at the top of the weld; positive on one side and negative on the other.

Undeformed

Deformed by horizontal shock load

Deformed by vertical shock load

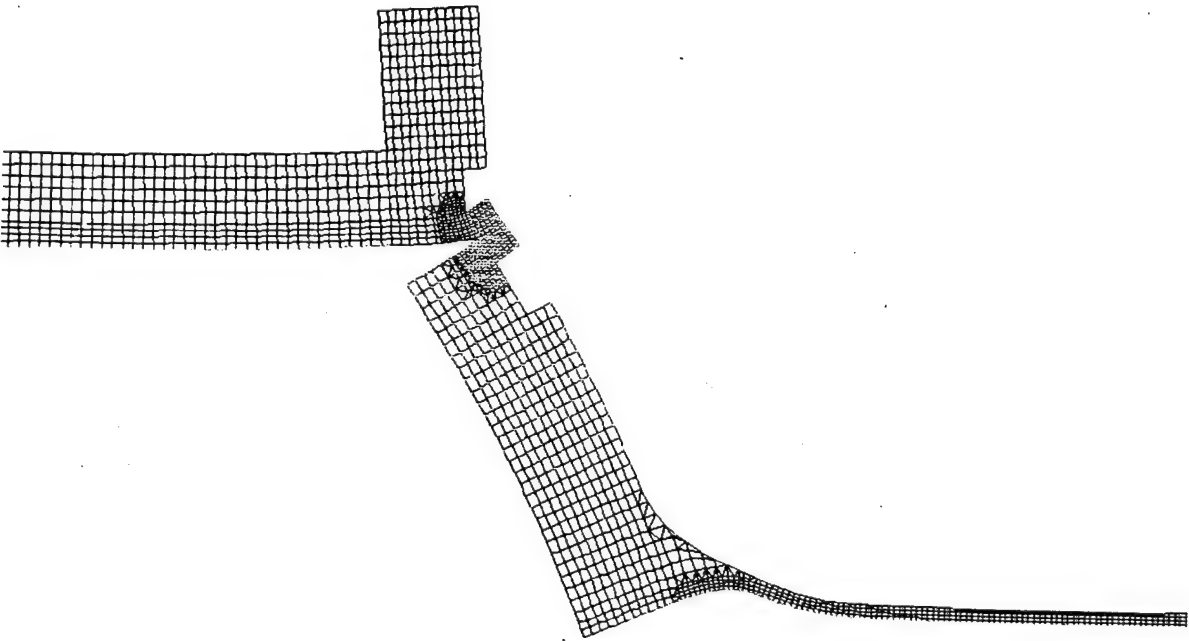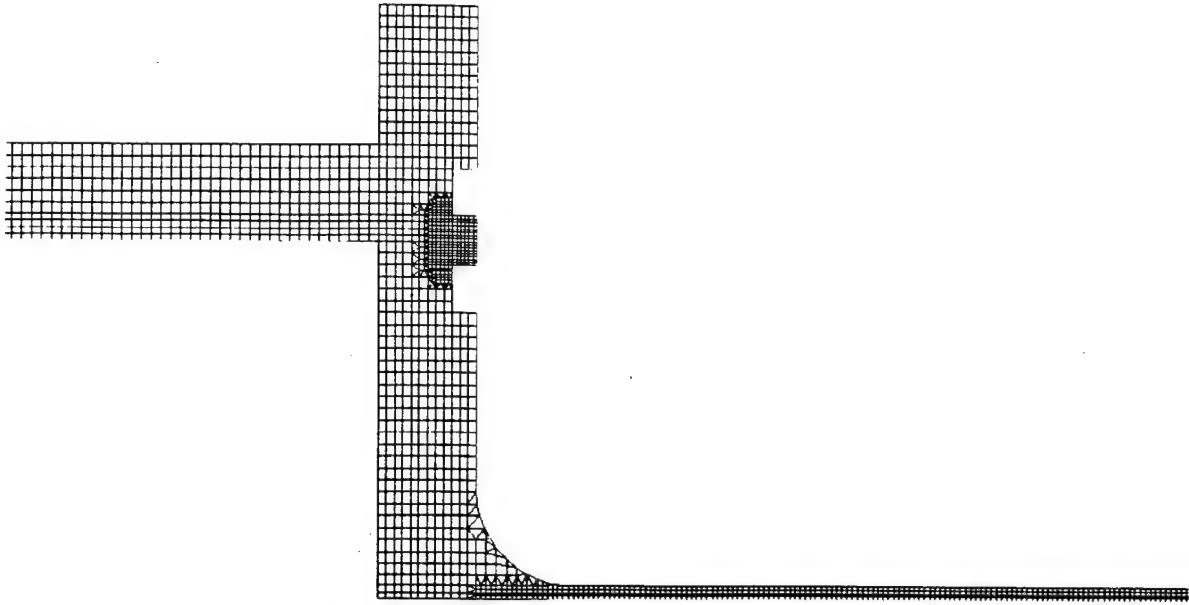Figure 6. Undeformed Plot and Deformed Plots for the Two Shock Loads

19

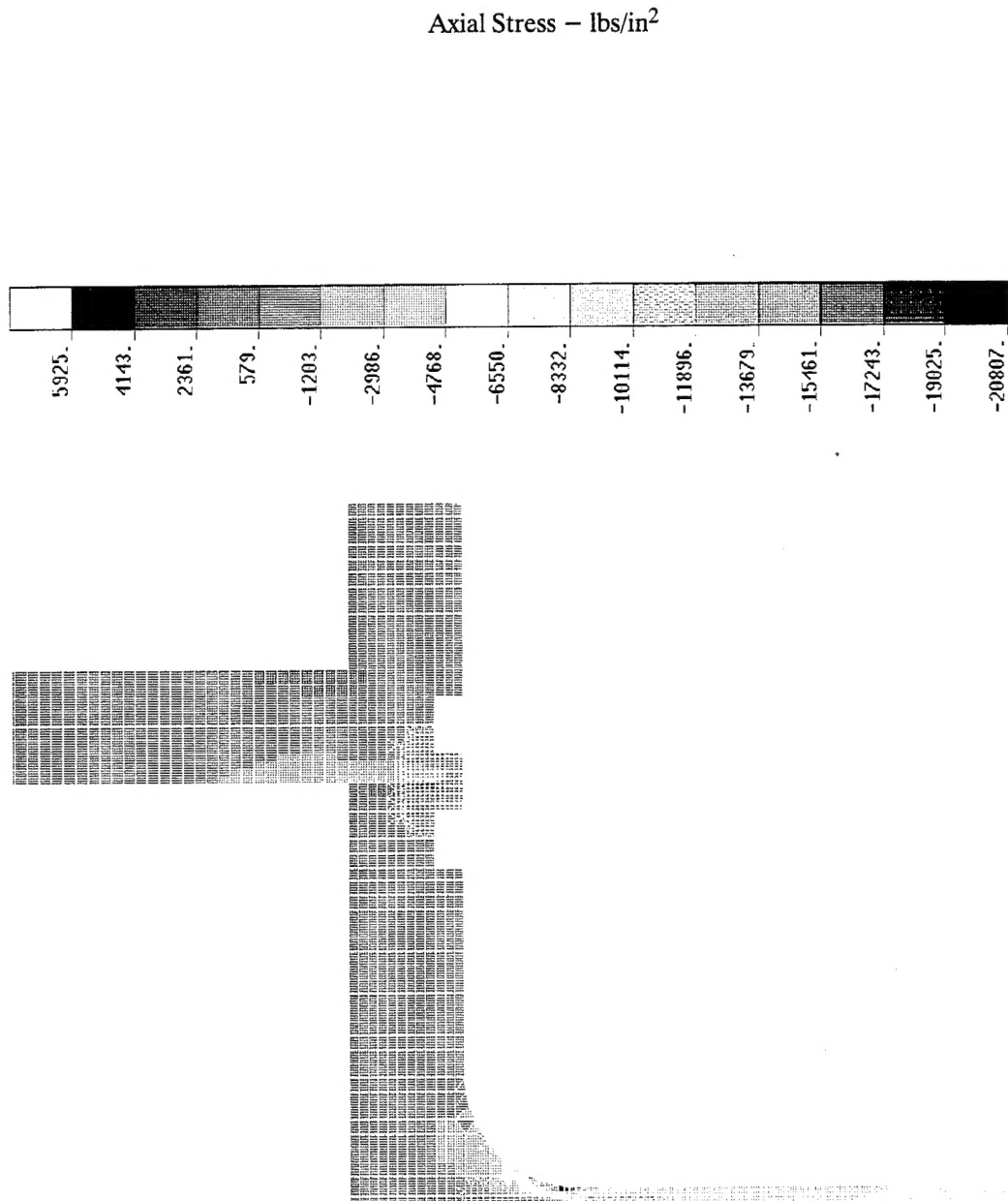Figure 7. Undeformed and Deformed Displacement Plots for Lower End of Stage One

Axial Stress – lbs/in^2

Figure 8. Stress Plot for Horizontal Acceleration
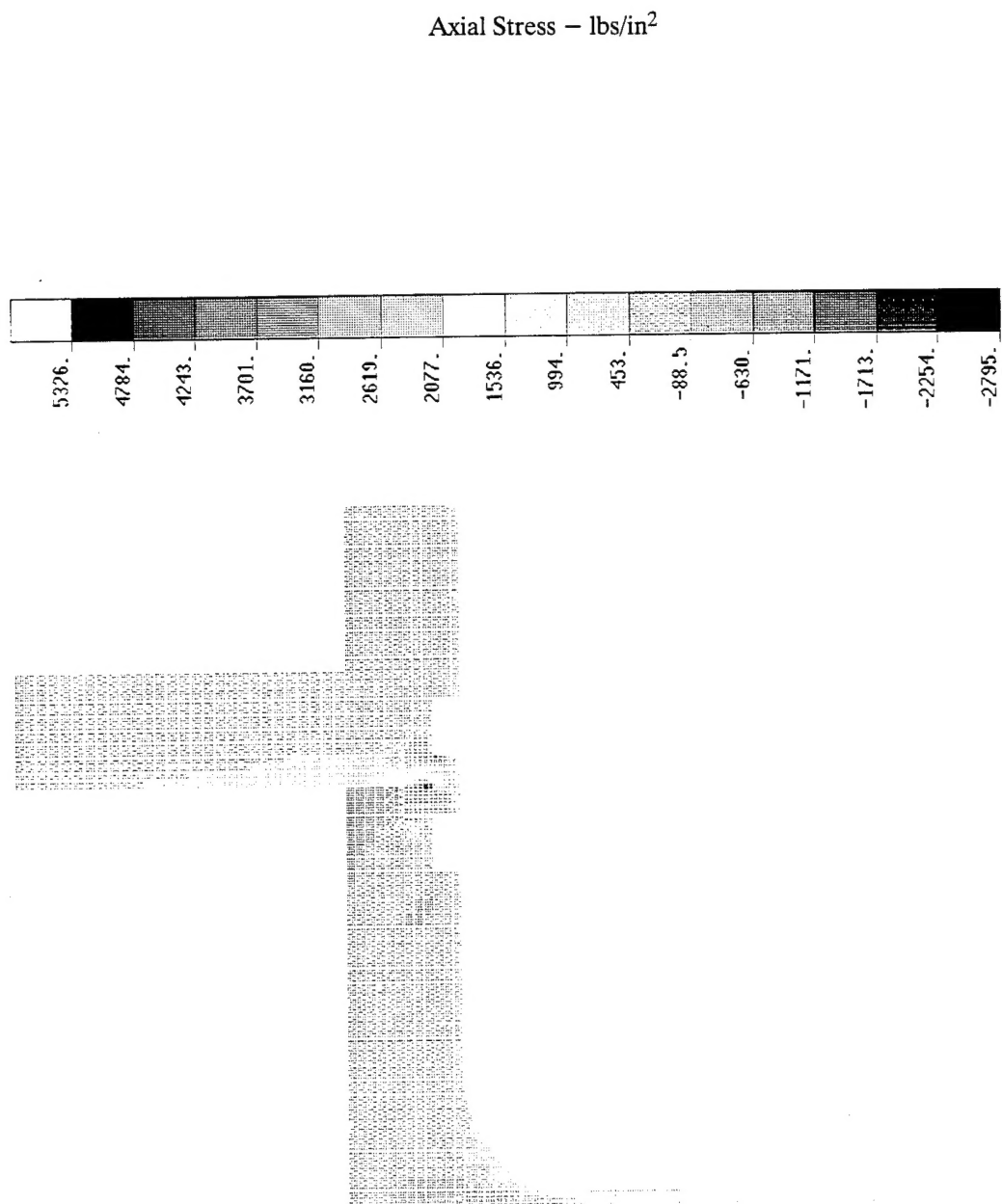
Axial Stress – lbs/in^2

Figure 9. Stress Plot for Vertical Acceleration

22

REFERENCES

1. Golda, M.E., Walters, J.D., and Green, G., "Applications of Superconductivity to Very Shallow Water Mine Sweeping," *Naval Engineers Journal*, vol. 104, pp 53–64, (1992).

2. Chafe, J., Green, G., and Reidy, R., "Neodymium Regenerator Test Results in a Standard Gifford-McMahon Refrigerator," *Proceedings of the 7th International Cryocoolers Conference*, Sante Fe, NM, pp 1157–1164 (1992).

3. Schwatzberg, F.R., et al, *Cryogenic Materials Data Handbook*, The Martin Company, Denver CO, (1964).

4. MacNeal, R.H., ed., "The NASTRAN Theoretical Manual", NASA SP-221(01), Washington, D.C. (1972).

5. Brady, G.S. and Clauser, H.R., *Materials Handbook*, Eleventh Edition, McGraw-Hill, New York (1979).

6. Bradley, T.L. Jr., Davies, T.M., McCampell, S.L., and Ykema, J.I., "Comparison of Shock Test Methods of MIL-S-901 Derived from Tests on a Circuit Breaker and Switchboard," *Naval Engineers Journal*, pp 178–190, (1992).

INITIAL DISTRIBUTION

Copies

2	ONR
1	4524(J. Gagorik)
1	(W. Chang)
1	PMO
1	407–4(C. Merlihan)
4	Coastal Systems Station
2	2120(Buhl)
1	2120(Nye)
1	2120(Bond)
1	Naval Academy/Lib
1	NRL (Tech. Lib.)
12	DTIC
1	Vector Research Co/E. Roth

CDNSWC DISTRIBUTION

Copies	Code	Name
1	20	
1	204	
1	2040.1	Everstine
1	2041	
1	2042	
5	2042	Schroeder
1	80	
1	81	
2	812	
2	812	Chafe
2	812	Dunnington
1	812	Fikse
1	812	Golda
5	812	Green
1	812	Walters
1	342.1	TIC
1	342.2	TIC